https://doi.org/10.1016/j.engstruct.2019.01.049

Superelastic NiTi SMA cables: thermal-mechanical behavior, hysteretic modelling and seismic application

Cheng Fang [a], Yue Zheng [a, b*], Junbai Chen [a], Michael C H Yam [c], Wei Wang [a]

[a] *College of Civil Engineering, Tongji University, Shanghai 200092, China*

[b] *Department of Civil and Environmental Engineering, University of California, Berkeley, CA, USA*

[c] *Department of Building & Real Estate, The Hong Kong Polytechnic University, Hung Hom, Kowloon, Hong Kong, China*

** Corresponding author: email: yzheng@tongji.edu.cn, Tel: +86 (0)21-65982926*

Abstract: This paper reports a comprehensive study on the mechanical behavior, annealing (heat treatment) scheme, hysteretic modelling strategy, and potential seismic application of superelastic shape memory alloy (SMA) cables. The study commenced with thermal-mechanical characterization of monofilament SMA wires, and in particular, the influence of annealing scheme on the mechanical and phase transformation characteristics of the material was revealed. A series of 7×7 SMA cable specimens were subsequently tested at room temperature under various cyclic loading protocols. It is observed, among other findings, that the SMA cables are able to reasonably "scale up" the satisfactory properties of the SMA wires, and the mechanical behavior of the SMA cables may be improved by annealing. A moderate annealing temperature and duration (i.e., 350-400 °C for 15 minutes) can generally increase the stiffness, energy dissipation, and form setting ability of the SMA cables considered in this study, whereas an overly high annealing temperature tends to compromise these characteristics. Following the experimental study, an effective numerical modelling approach is proposed which reliably captures the basic mechanical behavior of the SMA cables. A prototype bridge, where SMA cables are adopted as restrainers, is finally designed and analyzed to demonstrate the efficiency of the SMA components for seismic damage mitigation. The analysis result shows that the SMA-cable restrainers can effectively control the peak and residual displacements of the bridge girder, and make the bridge more resilient.

Keywords: superelastic shape memory alloy (SMA); cable; annealing (heat treatment); self-centering; seismic resilience; bridge restrainer

1. Introduction

Since initially developed in the 1960s, shape memory alloys (SMAs) have been successfully commercialized in the biomedical, electrical, automotive, aerospace, and oil industries [1]. Driven by the growing demand for more adaptive, resilient, and high-performance structural systems, SMAs have also attracted considerable attention among the community of civil engineers and researchers [2]. As a result of a solid-to-solid transformation between austenite (A) and martensite (M) phases with a possible intermediate phase called rhombohedral (R) phase, SMAs possess two well-known characteristics, namely, shape memory effect (SME) and superelasticity (SE) [3]. SME takes place when the SMA is stressed at a temperature below the martensite finish temperature M_f, where a residual strain occurs upon unloading but this permanent strain can be fully recovered when the temperature later increases above the austenite finish temperature A_f. On the other hand, SE is exhibited when the SMA is stressed at a temperature above A_f, where the induced strain can be recovered immediately upon unloading. The demarcation temperature between the two phases, e.g. A_f, can vary with different chemical compositions and manufacturing/annealing procedures for the material. Both the SME and SE have found their potential applications in the construction industry, although the latter has received more attention from the community of seismic engineers [4-10]. The basic stress-strain responses of SMA are illustrated in Fig. 1, where the SE is the focus of the present study.

Monofilament SMA wires are one of the most widely used SMA products because of their superior mechanical property, high performance efficiency, well-established manufacturing process, and wide availability in market. The cost of SMA wires has also been decreased significantly over the past decade. The fundamental thermal-mechanical behavior of superelastic SMA wires have been extensively studied [11-13], where flag-shaped stress-strain responses with satisfactory self-centering ability, energy dissipation, and cyclic repeatability were typically found. However, gripping (end-fixing) is a major challenge for SMA wires. In addition, the load resistance of SMA wires is inadequate for civil engineering applications, a fact which leads to most of the existing investigations on SMA wire-based devices being laboratory scale. This issue is also shared by SMA helical and Belleville washer springs where the material capacity is not fully mobilized [14-15]. SMA bars could

provide larger load resistance for engineering structures, but some studies revealed that they have inferior mechanical properties in comparison with SMA wires due to an increased difficulty in controlling cold work and annealing procedures [12]. Moreover, SMA bars are normally machined to the bolt form which can be vulnerable to fracture over the threaded section [16]. More recently, SMA ring springs have been developed which were shown to exhibit satisfactory load resistance and energy dissipation [17-18]. The research is still in its infancy and some technical issues such as manufacturing difficulty and friction surface treatment need to be further addressed.

As a newly emerged family member of SMA elements, SMA cables combine the advantages of conventional steel cables with unique mechanical properties thanks to the SE (or SME). A structural cable typically consists of a group of helically laid strands which are bundled assemblies of helically wrapped monofilament wires. SMA cables are able to reliably "scale up" the satisfactory properties of SMA wires with stiffness and strength better meeting the civil engineering requirement. In contrast to SMA bars, SMA cables are more cost effective and easy to handle and spool, and are adequately stiff in uniaxial tension whereas having no buckling issue in compression. The failure mode, featured by successive rupture of the wires, is less radical than SMA bars which fail in a brittle manner. This makes SMA cables more ductile and robust against accidental loadings. Furthermore, the construction of the SMA cables is very flexible with diverse helix angles and layups, catering to different design purposes.

Compared with other SMA products such as wires and bars, SMA cables are new and less explored, and the research started relatively late. Reedlunn et al. [19] carried out an experimental study on superelastic SMA cables with different types of layup, and found that a 7×7 construction could lead to mechanical responses comparable to those of monofilament wires. Similar studies were later carried out by Ozbulut et al. [20] and Sherif and Ozbulut [21], where the focus was on the fatigue characteristics. Carboni et al. [22] established a phenomenological model for SMA cables, and the prediction agreed well with test results. Biggs and Shaw [23] experimentally characterized the SMA cable actuators under repeated thermal cycles, and it was again confirmed that a 7×7 construction reasonably scales up the adaptive property of SMA wires. Mas et al. [24] presented the

potential application of SMA cables for reinforced concrete structures. Pull out tests were conducted to examine the bonding strength between the cables and the surrounding concrete, and small-scale concrete beams with SMA cable reinforcement were physically tested. In parallel to those experimental works, numerical studies were performed to further explore the application fields such as high-rise towers [25] and bridge bearings [26].

This paper provides further insight into the thermal-mechanical behavior of superelastic SMA cables, with particular focus on the influences of varying annealing schemes on their phase transformation temperature, strength, stiffness, hysteretic behavior, self-centering capability, energy dissipation, and form setting characteristics, which are essential for civil engineering applications. Following the experimental study, an effective numerical modelling approach is proposed which reliably captures the superelastic behavior of the SMA cables. To demonstrate the efficiency of the SMA cables for seismic damage mitigation, a prototype bridge employing SMA cables as restrainers to gain resilience is finally designed and analyzed.

2. Thermal-mechanical characterization of SMA wires

2.1 Material

Before a detailed discussion of the behavior of SMA cables, the basic thermal-mechanical property of monofilament SMA wires is first described in this section. The SMA wires investigated in this study are made of commercial Ti-50.8at.%Ni, i.e. 50.8% atomic percentage of nickel with the balance contributed by titanium. Following the melting process within a vacuum mid-frequency induction furnace, the alloy was processed by hot-working at 800-900 °C to reduce the size (e.g., diameter) of the starting cast ingot and to set up homogenization microstructure. The SMA ingot was further hot-worked at 600-700 °C, and then cold-worked (with a reduction ratio of 30-40% of the cross-sectional area) and straightened (450 °C for 30 seconds) to a final required diameter.

The as-received SMA wires can be further annealed to optimize some engineering demanding properties. The importance of annealing lies in the precipitation of Ti3Ni4 within the microstructure. The existence of the Ti3Ni4 precipitates can enhance the mechanical properties of SMA products by

facilitating the martensitic transformation and hindering plastic flow in the surrounding austenite matrix [27-29]. The annealing process could also change the transformation temperatures, and in addition, affect the form setting behavior of the SMA. In practice, the annealing protocol, which is often a trade secret, is of particular interest to engineers who look for optimum SE or SME functions offered by the SMA products.

2.2 Transformation temperatures

The transition from Austenite (A) to Martensite (M) phases is called forward transformation, and that from M to A phases is called reverse transformation. There are four characteristic temperatures that are associated with the transformation processes, namely, martensitic start temperature M_s, martensitic finish temperature M_f, austenite start temperature A_s, and austenite finish temperature A_f. The transformation temperatures of SMA are important parameters because their location relative to the testing/working environment (e.g., room temperature) determines if the material will exhibit SE or SME (or neither) behavior. As mentioned, SMA fully exhibits SE when the temperature is above A_f, and fully exhibits SME when the temperature is below M_f.

A series of 0.8 mm-diameter SMA wires were annealed at different temperatures (ranging from 350-550 °C) for different durations (ranging from 5-30 minutes). These wire samples were annealed together with the SMA cable specimens in an electrical furnace and then water quenched. After annealing, Differential Scanning Calorimeter (DSC) testing was employed to obtain the transformation temperatures of the SMA wire samples. DSC captures heat flow with continuous changes of temperature of the material, and provides an indication of the associated transformation temperatures as the material goes through endothermic and exothermic solid-state phase transformations. Each sample material was loaded into the DSC machine and subjected to a cooling-heating cycle with a rate of 10 °C/minute.

Fig. 2(a) shows the DSC curves of the various wire samples after being subjected to different annealing schemes. The phase transformation start and finish temperatures can be determined based on the onset points (toes) of the peaks in the DSC curve, as illustrated in Fig. 2(b). It is noted that not all the peaks in the DSC curves are easily identified, and the pattern depends on various factors

including the alloy's chemical composition, annealing scheme, and the history of mechanical deformation [30]. A single peak in the heating or cooling DSC curve indicates that the alloy experiences phase transformation without passing through the R phase, in which case the toes of the peaks correspond to the representative transformation temperatures, i.e., M_s, M_f, A_s, and A_f. In some cases two successive peaks are seen in the cooling or heating cycle (or in both procedures), and such pattern indicates the existence of an R phase between the M and A phases.

The results show that the as-received sample (receiving no annealing) experiences two-stage forward (cooling cycle) and reverse (heating cycle) transformations. The forward transformation starts at approximately 15 °C, and the entire transformation process is finished at a temperature lower than -100 °C. The reverse transformation is finished at around 19 °C, above which the material is in the A phase. With increasing annealing temperatures, the transformation temperatures of the material first increase slightly and then decrease. This trend is generally in line with that reported in other independent studies [30-31]. Another phenomenon is that the two-stage transformation peaks gradually merge into a single peak when the annealing temperature increases. In addition, an increase in the annealing temperature, which tends to release the internal stress fields and dislocations, could make the peaks more remarkable [30].

When the superelastic property of the SMA wires is to be utilized, as would be the case for the current study, the A_f should be lower than the room temperature. For the SMA wires experiencing the different annealing schemes considered in this study, the A_f can be shifted by nearly 50 °C, where the highest value is around 30 °C (i.e., sample annealed at 350 °C for 30 minutes) and the lowest value is around -20 °C (i.e., sample annealed at 550 °C for 5 minutes). For most cases, the A_f is lower than the room temperature (28 °C). From a practical application point of view, a desirable A_f can be achieved by either adjusting the chemical compositions, or by changing the annealing schemes. The former approach can be easily done by material suppliers (material engineers), and civil engineers are capable of doing the latter. When an improved mechanical property of the SMA is desired and concurrently a sufficiently low A_f is required, a combination of the two approaches may be used.

2.3 Mechanical properties

The typical cyclic stress-strain responses of the monofilament SMA wire samples are shown in Fig. 3. For the as-received wires and those receiving a moderate annealing temperature (i.e., 400 or 450 °C for 15 minutes), recognizable flag-shaped responses with satisfactory recoverability are exhibited, although certain degradations of the transformation plateau accompanied by an accumulation of residual strain are observed. This phenomenon is called Transformation Induced Fatigue (TIF), which is common in commercial superelastic SMA [3, 32]. These wires are shown to exhibit good recoverability with a residual strain of less than 0.5% after undergoing an 8% maximum strain, indicating a recovery rate of more than 90%. When a higher annealing temperature of 500 °C is applied, however, the hysteretic behavior of the wire starts to deteriorate, implying that the sample may be over aged. Frick et al. [27] confirmed that over aging leads detrimental effects on the strain recovery property of SMA.

The characteristic parameters of superelastic SMA (see Fig. 1) can be extracted from the stress-strain curves. Considering the non-annealed sample for example, the approximate values of the key parameters are: forward transformation start stress ("yield" strength) $\sigma_{Ms} \approx 510$ MPa, forward transformation finish stress $\sigma_{Mf} \approx 600$ MPa, reverse transformation start stress $\sigma_{As} \approx 270$ MPa, reverse transformation finish stress $\sigma_{Af} \approx 200$ MPa, and Young's Moduli ($E_A \approx 50$ GPa and $E_M \approx 30$ GPa). The maximum transformation strain, $\varepsilon_L \approx 5\%$, is obtained by constructing a reverse extension line based on the unloading path from σ_{Mf}.

3. Test program of SMA cables

3.1 Cable specimens

A 7×7 cable construction was considered, as shown in Fig. 4. Each cable specimen was prepared with a total length of approximately 350 mm, and consists of seven helically wrapped strands, each consisting of seven helically wrapped monofilament SMA wires of 0.8 mm diameter. This arrangement leads to a measured outer cable diameter of around 7 mm. The different specimens were cut from the same coil of cable, and the two ends of each specimen were firmly constrained to avoid unravelling. The specimens were then annealed via an electrical furnace at different targeting

temperatures for varying durations, as summarized in Table 1. All the SMA cable specimens were virgin without being trained before the cyclic tests.

3.2 Test arrangement

The cable specimens were uniaxially loaded via a Universal Test Machine (UTM), as shown in Fig. 4. The ends of the cable were coated with a thin layer of epoxy to avoid stress concentration, i.e., to avoid damage to the gipped part due to high clamping force. The ends were rigidly clamped by the top and bottom hydraulic wedge grips that match the external diameter of the cable. The load was recorded by a built-in load cell of the UTM, and the stress of the cable was calculated by dividing the load by the sum of the cross-sectional area of the 7×7=49 monofilament wires. The global strain ε_g was determined by the grip displacement, i.e., $\varepsilon_g = \Delta L/L_{eff}$, where ΔL is the axial elongation of the cable which is controlled by the UTM, and L_{eff} is the free length of the cable between the two grips. Local strain-field near the mid-length region was monitored simultaneously by a GOM Digital Image Correlation (DIC) camera. DIC is an optical, non-contact double-camera technique that measures surface displacements of an object by tracking the specular pattern on the surface of a specimen [33]. It independently provides full field strain data, with a sampling frequency taken as 0.5 Hz in this study, i.e., one photograph per two seconds. The DIC images were analyzed using the GOM commercial software after the tests, and the main output data of interest is the local strain field within the monitored region. To facilitate object seizure, the surface of the cable was treated with paint spraying using white background and irregular black dots. Physical extensometer was found to be unsuitable for such experiment as the bending deformation of the cable during the unloading process could cause slippage of the clamping legs and thus making the measurement unreliable.

Two different loading protocols, namely, cyclic loading with incremental strain and cyclic loading with constant strain, were considered for the test program. For the former case, the loading process starts with a 1% initial strain and proceeds with a 1% strain incremental interval until 10% strain. Two cycles were repeated at each strain level. For the latter case, a constant strain amplitude was applied and was repeated for 20 times. A strain amplitude of 6% was typically considered, but

some selected specimens were subjected to a constant strain amplitude of 10%. It is believed that these loading protocols can adequately demonstrate the hysteretic behavior of the cables under seismic excitations. Displacement control with a constant loading rate of 5 mm/min was employed, and all the tests were conducted at a room temperature of approximately 28 °C.

For ease of identification, each cable specimen was designated with a test code that starts with the annealing temperature and duration (NA indicates no annealing), followed by the loading protocol (I= incremental and C = constant). A final letter "d" means duplicate test. For instance, specimen 350-15-C6 means that the cable was subjected to a 350 °C annealing temperature for 15 minutes; the loading protocol was "constant cyclic loading" with a strain amplitude of 6%.

3.3 Test results

All the cable specimens experienced anticipated axial elongations with no failure during the entire loading procedures. With increasing loading cycles, lateral "bending" was observed when the grip displacement returned to zero, but this slack deformation quickly vanished when the applied load was regained. This phenomenon is attributed to the accumulated residual strain which leads to a permanent cable elongation.

The global stress-strain responses of the cable specimens under the incremental or constant strain cyclic loading are shown in Fig. 5. For the non-annealed cable specimens, flag-shaped behavior with satisfactory strain recoverability are generally shown, although the "yield" strength and transformation plateaus are less recognizable than those observed in the stress-strain curve of the corresponding monofilament SMA wire. Similar findings were also reported in other studies [19-21, 24]. The relatively smooth stress-strain behavior of the SMA cables is attributed to their bundled construction, where different wires in the cable are loaded in different and complex deformation modes (including a combination of tension, torsion, and bending) with diverse stress distributions. As a result, the axial load is not uniformly shared among different wires, and some wires undergo forward transformation earlier than the others. The non-synchronization of stress development leads to a more gradual evolution of the total stress-strain responses of the cables [24, 34].

Similar to the behavior of monofilament SMA wires, certain degradations of the yield strength accompanied by an accumulation of residual strain are observed in the SMA cables. More remarkable degradations are induced for the specimens subjected to a larger strain amplitude (e.g., NA-C6 versus NA-C10). It is believed that the residual strain is mainly from two sources, i.e., TIF of the material itself as well as structural relaxation. The latter is a common phenomenon observed in almost all kinds of cables. While it is difficult to tell the exact proportions of the contributing factors, a proper training can mitigate both effects. This can be particularly confirmed by observing the stress-strain curves of the specimens subjected to constant strain cyclic loadings, where the first loading cycle leads to the most evident residual strain, whereas the hysteretic response becomes stabilized in the subsequent loading cycles.

Importantly, the SMA cables do exhibit dependence on the annealing scheme. More recognizable flag-shaped behavior are shown for the specimens receiving an annealing temperature below 450 °C. Compared with the non-annealed specimens, these annealed specimens seem to exhibit more distinguishable "yielding" strength and transformation plateaus, and in addition, slightly "wider" hysteretic loops. This may be related to the form setting property (as elaborated later) of the annealed cables, and as a result the constituent SMA wires are "stiffer" and tend to resist the load in a more uniform fashion.

Being consistent with the test results of the monofilament SMA wires, the cables receiving a higher annealing temperature of 500 or 550°C show a typical "over aging" behavior with more evident degradation and more pronounced accumulation of residual strain. Apart from the possible deterioration of the SMA material itself, the significantly shifted transformation temperatures could also be a factor attributing to the less satisfactory hysteretic behavior. As can be seen from Fig. 2, the austenite finish temperature (A_f) abruptly decreases from around 15 °C to as low as -20 °C when the annealing temperature increases from 450 °C to 500 °C. In other words, for the cables receiving an annealing temperature of 500 °C or above, the room temperature was more than 45 °C higher than A_f. The effect of varied environmental temperatures on the superelastic behavior of SMA has been studied by a number researchers [3, 14], and it was concluded that the room/working temperature of

SMA should preferably fall within the range between A_f and A_f +40 °C to ensure a proper SE. A further increase in the working temperature may cause an increased amount of plastic (permanent) strain, and when the room temperature exceeds the maximum possible temperature for phase transformation (this temperature is often designated as M_d), the required forward transformation stress finally exceeds the true yield (plastic) stress of the material, and as a result the SE is completely lost.

The local strain field obtained from the DIC is generally consistent with the global strain, as typically shown in Fig. 6. The DIC strain contour indicates that the local strains can slightly vary at different locations of the cable, which could be due to the "non-uniform" texture of the cable surface. A representative local strain can be derived by randomly selecting a series of points (normally more than 10 points) along the length of the cable at regular intervals and then obtaining the average value. Using this way, the obtained average DIC strain history is shown in the figure. Clearly, the local strain follows the predefined loading protocol, although the DIC strain values tend to be slightly smaller than the global strain. One possible explanation is that a higher local strain occurs near the gripped ends of the cable [20], but these stress concentration areas are beyond the DIC monitored region in the present study. In addition, even though no visual slippage at the clamped ends of the cable was observed, minor slippage is in fact inevitable in such test setup [19], especially at large strain levels. Nevertheless, the difference of the DIC and global strains is typically less than 5%, and therefore, the use of global strain can adequately represent the overall stress-strain responses of the cables from an engineering point of view.

4. Discussion of test results

4.1 Form setting property

Form setting (shape setting) refers to the process used to form a SMA product into a specific and often complex geometric component [35]. This is often realized by temporarily constraining the material into a new desired shape and then performing a form set annealing process followed by water quenching. In fact, annealing and form setting are often intentionally done simultaneously. For

practical use of SMA cables, it may be necessary to maintain the twisted form and to avoid unwinding at room temperature, unless reliable end constraints are permanently applied to the cables.

In order to examine the influence of the annealing scheme on the form setting ability of the SMA cables, the cable specimens were cut from the mid-length after the cyclic test. As clearly shown in Fig. 7, no form setting ability is observed for the non-annealed specimen, and as a result the cable completely unraveled after the cutting. Moderate form setting ability is gained for the specimens subjected to an annealing temperature of 350 °C, where partial unravelling near the cutting location is observed. Enhanced form setting ability is enabled when the annealing temperature increases to 400-500 °C for 15 minutes. The results indicate that in order to avoid unravelling and thus to make the SMA cables easier to handle, an annealing temperature of 400 °C or above for 15 minutes is generally adequate.

4.2 Strength and stiffness

Figs. 8(a) and 8(b) show the "yield" strength and peak stress of the SMA cable specimens as a function of cycle numbers. The yield strength is estimated as the intersection of the two extension lines along the initial elastic and inelastic plateau paths of each cycle, as illustrated in Fig. 8(a). Due to the various sources of degradation, the yield strength keeps decreasing with the arrival of new incremental loading cycles; on the other hand, the constant cyclic loading scenario leads to the most evident decrease of the yield strength during the first few cycles and then the yield strength decreases mildly. This implies that the degree of degradation mainly depends on the historic maximum strain. In other words, the yield strength tends to be stabilized when the cable is trained within a certain maximum strain, and only after a "new" larger maximum strain is attained that a noticeable degradation is further induced. Although not very obvious, annealing temperatures of 350-400 °C seem to mitigate the degradation of the yield strength compared with the non-annealed cables. Clearly, an overly high annealing temperature (e.g., specimen 500-15-I) leads to more rapid decrease of the yield strength. It is observed that the yield strengths of the specimens at the final cycle (20^{th} cycle) are generally below 400 MPa, corresponding to at least a 20% reduction compared with the value at the initial cycle (approximately 500 MPa).

On the contrary, the peak stress, as shown in Fig. 8(b), keeps increasing with increasing incremental cycle numbers. The value is also quite stable throughout the entire constant cyclic loading process. These indicate that the peak stress of the SMA cables is not much influenced by the degradation phenomenon, and the ultimate load carrying capacity can be well maintained. This property could be essential for seismic applications where a reliable and adequate load resistance is required at large structural deformations. Again, the annealing scheme has a mild effect on the peak stress.

The stiffness response of the cables is more sensitive to the annealing scheme, as shown in Fig. 8(c). The initial elastic modulus of the cables ranges from 30 to 45 GPa, where a higher annealing temperature tends to cause an increased elastic modulus. This tendency is believed to be mainly related to the form setting property of the cables. In particular, the twisted wires undergoing form setting can provide extra stiffness when the cable is elongated, and these wires can be more closely interacted with each other after annealing. The change of the elastic moduli of the material itself due to the different annealing schemes could also attribute to the difference in the cable stiffness. In any case, for all the cable specimens, the elastic modulus decreases with increasing cycle numbers. It is noted that in practice, the SMA cables can be used in a prestrained state such that a much higher initial stiffness can be achieved.

4.3 Self-centering capability

Figs. 9(a) and 9(b) show the accumulated residual strains of the specimens as a function of cycle numbers under the incremental and constant cyclic loading, respectively. When subjected to incremental cyclic loading, the residual strain is gradually accumulated with an increase in the maximum strain. Except for specimen 500-15-I, the final accumulated residual strains for the cables are generally below 1.5%, corresponding to a recovery rate, i.e., ratio of the recovered strain to the maximum strain, of more than 85%. For specimen 500-15-I, the final accumulated residual strain is 3.3%, corresponding to a reduced recovery rate of 67%. This is in line with the less satisfactory stress-strain response of the wire as previously shown in Fig. 3.

When constant cyclic loading is applied, the residual strain is most quickly accumulated during the first loading cycle, and subsequently the development of residual strain starts to slow down. For most specimens, more than 80% of the final residual strain is developed within the first five cycles. According to the limited test data from this experimental program, it is suggested that for practical use of the SMA cables, a 'pre-training' with about five loading cycles at the target strain level may effectively stabilize the behavior of the cables and limit further development of residual strain. After 20 loading cycles at 6% constant strain, the recovery rate exceeds 83% for the specimens receiving an annealing temperature of no more than 450 °C, and a slightly lower recovery rate (i.e., 79%) is observed when the specimen is under an increased cyclic strain of 10%. Again, a higher annealing temperature of 500 °C deteriorates the self-centering capability. It can also be deduced from the test results that a prestrain (pretension) of at least 15% of the target maximum strain may eliminate the residual strain of properly annealed SMA cables during earthquake excitations.

4.4 Energy dissipation

In addition to the self-centering capability, the SMA cables can be employed for energy dissipation purposes (or at least to provide supplementary energy dissipation). The energy dissipation capability is presented by a dimensionless index, namely, equivalent viscous damping ratio (EVD), as defined by:

$$EVD = \frac{W_D}{4\pi W_E} \tag{1}$$

where W_D is the energy loss per cycle, which is essentially the area enclosed by a stress-strain hysteretic loop, and W_E is the strain energy stored in a corresponding linear system. For the current specimens, as shown in Figs. 10(a) and 10(b), the EVD ranges between 2% and 6%, depending on several factors including loading protocol, maximum strain, and annealing scheme. At the same maximum strain level, the specimens receiving an annealing temperature of 350-450 °C generally show higher EVDs than the non-annealed specimens, which echoes the wider hysteretic shapes of the former. Again, the increased EVD can be caused by the form setting behavior of the annealed

specimens. It is noted that due to the non-synchronization of stress development within the cross-section, the SMA cables exhibit smaller EVD values than the monofilament SMA wires which typically have an EVD of 7% or above.

5. Numerical investigations

Following the experimental study, a numerical modelling approach is developed to capture the superelastic behavior of the SMA cable specimens. A prototype bridge is then designed and analyzed to demonstrate the efficiency of the SMA cables against seismic hazard.

5.1 Modelling of SMA cables

Over the past two decades, the hysteretic behavior of SMA has been extensively studied and many constitutive models with different complexities have been developed [36-38]. Among these models, a simple one-dimensional (1D) flag-shaped hysteretic model is generally sufficient to catch most key characteristics of superelastic SMA [Eatherton et al. (2014)], as typically shown in Fig. 11. The flag-shaped model only requires a limited number of controlling parameters, which can be calibrated from the wire results. In this study, the numerical models are established using the open source program OpenSees [39]. A displacement-based fiber nonlinear element using a *Self-centering material* is employed to simulate the SMA wire. The cross section of the element is divided into six layers along radius direction and each layer is divided into 24 fiber elements around circumference. Fig. 11 shows the numerical simulation result of a typical SMA wire (annealed at 400 °C for 15 minutes) together with the test result. The basic parameters for the model are given in Table 2. It is shown that the characteristic stresses and strains from the numerical simulation correlate well with the test results, although the degradation effect is not taken into account in the numerical model.

While more complex hysteretic behavior is exhibited by the SMA cables compared with monofilament SMA wires, the modelling approach for the latter can still form the basis of the SMA cable model which should reflect the following extra characteristics: 1) less recognizable flag-shaped hysteresis is exhibited by the SMA cables due to out-of-sync tension of the constituent individual wires; 2) the SMA cables have less full hysteretic loops than the SMA wires; 3) the Young's

modulus and post-yield stiffness of the SMA wires are larger than those of the SMA cables; and 4) non-negligible degradations of the yield strength and forward transformation plateau are exhibited by the SMA cables. In order to consider these unique properties, an empirical hybrid modelling solution, namely, combined multi-layer SMA and steel fiber modelling approach, is developed and introduced herein.

As illustrated in Fig. 12(a), the cross-sectional area of all the 49 SMA wires in a SMA cable can be equivalent to an idealized circular section with a reduced diameter of 5.6 mm. The equivalent cross-sectional area is divided into several parts (four in the study) and each part is assigned with a particular type of material: the first part, which locates in the central region of the equivalent section, is assigned with an isotropic hardening steel material (*Steel02*) to mimic the permanent strain and degradation phenomena of the SMA cables. These soft steel fibers have the same yield strength as those of the SMA. The remaining three parts are all assigned with a *Self-centering material*, but with different initial Young's moduli using varying reduction factors (k_0) to consider the effect of out-of-sync tension of different groups of the SMA wires. The reduction factor is the ratio of the Young's modulus of a particular layer of SMA material to that of the monofilament SMA wire. The reduction factors (k_0) as well as the cross-sectional areas of the different parts may be determined via an error-and-trail process until a satisfactory agreement with the test results is achieved. It should be noted that there may be other combinations of these materials with different material properties and assigned areas to achieve similar results. Those combinations can also be used as long as they lead to good agreement with the test results.

The parameters adopted for a representative specimen (i.e., 400-15-I) are given in Table 3, and the resulting numerical prediction is shown in Fig. 12(b). It is seen that the shape of the hysteretic loop of the SMA cable is well captured by the proposed model, and the degradation of the yield strength is also reasonably reflected. However, some discrepancies still exist, especially along the unloading paths. While a refined simulation may be achieved by further adjusting the parameters in Table 3 (e.g., to optimize the values of β or cross-sectional areas of different material layers), no such effort is made as we believe that for demonstration purpose, the accuracy of the model is

sufficient and the discrepancy should have practically no tangible influence on the main conclusions obtained from the following case study.

5.2 Prototype structure

The unique self-centering and energy dissipation capabilities can motivate diverse applications of the SMA cables in seismic engineering. A case study is provided here which considers SMA cables as restrainers for bridges against strong earthquakes. To demonstrate the damage mitigation efficiency of the restrainers, a two-span continuous reinforced concrete (RC) girder bridge is designed and investigated. The topological layout of the bridge is shown in Fig. 13 (unit in cm). The RC girders are supported by two end abutments as well as a single central RC pier with a diameter of 1.4 m and a clear height of 8.0 m. The longitudinal and transverse reinforcement ratios of the RC pier are 1.25% and 0.2%, respectively. C30 concrete is used, and the yield strength of the reinforcing bars is 280 MPa. The elastic moduli of the reinforcement and the concrete are 2.0×10^5 and 3.0×10^4 MPa, respectively. The width of the expansion joint at the two abutments is 100 mm to allow free movement of the girder under service (i.e., braking, temperature) and accidental (i.e., earthquake) loads.

The length and number/size of the SMA cables may be selected in practice based on the following criteria: 1) the SMA cables stay elastic under the frequently-occurring earthquake (FOE); 2) the SMA cables don't go beyond the forward transformation plateau (e.g., strain being typically less than 8%) under the design-based earthquake (DBE); 3) the SMA cables don't advance into the plastic plateau under maximum considered earthquake (MCE); and finally 4) the SMA cables don't fracture under extremely rare events beyond the MCE. Based on the above criteria, a total of 100 SMA cable restrainers (50 for each direction) are installed between the two abutments and the RC girder, as well as between the bent cap and the girder, as shown in Fig. 13. The length of each SMA-cable restrainer is 300 mm, with a slack deformation (before load resistance is gained) of 60 mm to allow free movement of the girders under service loads. The SMA cables are assumed to be subjected to an annealing temperature of 400 °C for 15 minutes. This annealing scheme has been shown to improve the stiffness, energy dissipation, and form setting characteristics compared with

the non-annealed SMA cables. The SMA cables used for the prototype bridge have the same cross-sectional size as that of the test specimens. It should be noted that larger diameter cables can be used in practice, in which case the necessary number of restrainers can be significantly decreased. However, this needs further calibration studies against available test results.

5.3 Modelling of prototype bridge

A finite element (FE) model of the prototype bridge is established in OpenSees. Fig. 14(a) shows the schematic model together with the detailed modeling information. The RC girder and the abutments are modeled using linear elastic beam-column elements. Frictional sliding bearings are placed on the bent cap and the two abutments. These bearings are modeled by zero-length spring elements, where the initial elastic stiffness and the frictional coefficient are taken as 123.0 kN/mm and 0.03, respectively. An ideal *elastic-plastic material* is used to simulate the behavior of the frictional bearings. The RC pier is modeled by displacement-based nonlinear fiber elements which account for the nonlinear characteristics of both concrete and reinforcement. Each element consists of three types of hysteretic material model, namely, reinforcement, confined concrete, and unconfined concrete. The hysteretic behavior of the reinforcing bars is represented via a uniaxial Menegotto-Pinto constitutive model with the linear kinematic hardening and aero isotropic hardening [40]. The uniaxial Kent-Scott-Park concrete model [41] is used to simulate the unconfined and confined concrete. The soil-structure interaction (SSI) effect of the soil-pile-foundation is taken into account by introducing several zero-length spring elements at the bases of the abutments and pier. Details of the SSI simulation can be found elsewhere [42].

The 50 SMA cable restrainers in each direction are modeled by a lumped nonlinear displacement-based fiber element plus a zero-length gap element in series, as shown in Fig. 14(b). The gap element, allowing a free displacement of 60 mm, is used to consider the slack effect which is important because the bridge girders can move with a non-negligible displacement due to the change of environmental temperature. The other parameters of the SMA-cable restrainers are the same as those considered for the SMA cable specimen discussed previously.

5.4 Behavior of bridge with SMA cable restrainers - an illustrative example

To demonstrate the effectiveness of the SMA-cable restrainers, an illustrative nonlinear time-history analysis on both the traditional bridge (i.e., that without the SMA-cable restrainers) and the novel bridge with the SMA-cable restrainers is performed. The unscaled El Centro (EW) earthquake record is used as the external excitation, where the accelerogram is shown in Fig. 15(a). The peak ground acceleration (PGA) of the ground motion is 0.214g. The girder displacement responses of the traditional and novel bridges under the selected earthquake record are displayed in Fig. 15(b). It is shown that the peak girder displacement in the traditional bridge is significantly larger than that of the novel bridge. Importantly, the residual girder displacement is significantly decreased when the SMA-cable restrainers are used. The total hysteretic behavior of the SMA cable restrainers is presented in Fig. 15(c). As expected, the slack restrainers first undergo a free displacement before getting tightened. The maximum elongations (excluding slack) of the lumped SMA-cable restrainer springs at the left and right abutments are 16 mm and 25 mm, respectively, corresponding to strains of 5.3% and 8.3%. According to the test results, the SMA-cable restrainers work within a safe strain range. Generally speaking, the SMA-cable restrainers are shown to effectively control the peak and residual displacements of the girder, and as a result can help mitigate bridge damage and enhance structural resilience. More ground motions should be considered in further studies, and a performance-based design framework may be developed in future. These are beyond the main focus of this study.

6. Summary and conclusions

This paper has provided insight into the thermal-mechanical behavior and seismic application of superelastic SMA cables, with particular focus on the influences of varying annealing schemes on the phase transformation temperature, strength, stiffness, hysteretic behavior, self-centering capability, energy dissipation, and form setting characteristics of the cables. A simple yet effective numerical modelling approach was proposed which has been found to reliably catch the fundamental mechanical behavior of the SMA cables. A prototype bridge structure employing SMA cables as

restrainers is finally designed and analyzed to demonstrate the efficiency of the SMA cables for seismic mitigation. The main findings and conclusions are as follows:

- At monofilament wire level, the thermal-mechanical behavior of the SMA is sensitive to the annealing history. With increasing annealing temperatures, the transformation temperatures of the material first increase slightly and then decrease. The SMA wires generally show stable flag-shaped hysteretic responses with excellent self-centering capability, but an overly high annealing temperature (e.g., 500 °C or above) tends to deteriorate the mechanical performance of the SMA.
- The 7×7 SMA cables are able to reasonably scale up the satisfactory properties of the SMA wires, although a more gradual evolution of the stress-strain responses is observed due to the complex deformation modes and stress states of the different individual wires within the cable.
- Form setting can be stimulated by the annealing process. A "full" form setting ability is promoted for the SMA cables when the annealing temperature reaches 400 °C or above for 15 minutes followed by water quenching. A lower annealing temperature leads to partial form setting.
- The yield strength of the SMA cables tends to decrease with increasing cycle numbers, but the hysteretic loop can be stabilized with a few training cycles. Increasing the annealing temperature can increase the stiffness of the cables, but has a less pronounced influence on the strength characteristics.
- The recovery rate exceeds 80% for most SMA cable specimens. Being consistent with the behavior of the SMA wires, an annealing temperature of 500 °C or above can compromise the self-centering capability.
- The EVD of the SMA cable specimens ranges between 2% and 6%, depending on loading protocol, maximum strain, and annealing scheme. An annealing temperature ranging from 350 to 450 °C can help enhance the energy dissipation capacity.
- The combined multi-layer SMA and steel fiber modelling approach proposed in this study is shown to well capture the superelastic behavior of the SMA-cable specimens. The case study on a prototype bridge confirms that the SMA cables can be used to mitigate the seismic damage to bridges.

7. Acknowledgements

The financial support from the National Natural Science Foundation of China (NSFC) with Grant Nos. 51778456 and 51778459 is gratefully acknowledged. The natural science foundation of the Shanghai Pujiang Program under grant number 16PJ1409600 is also gratefully acknowledged. The authors would also like to express their gratitude to Weikang Feng, Dong Liang, and Jin Zhao for assistance with the cable surface/gripped end treatments as well as data processing.

8. References

[1] Jani JM, Leary M, Subic A, Gibson MA. A review of shape memory alloy research, applications and opportunities. Materials and Design 2014;56:1078-1113.

[2] Chang WS, Araki Y. Use of shape-memory alloys in construction: A critical review. Proceedings of the Institution of Civil Engineers: Civil Engineering 2016;169(2):87-95.

[3] Lagoudas DC. Shape memory alloys: modeling and engineering applications. Springer, USA, 2008.

[4] Fang C, Yam MCH, Lam ACC, Xie LK. Cyclic performance of extended end-plate connections equipped with shape memory alloy bolts. Journal of Constructional Steel Research 2014;94(94):122-136.

[5] Yam MCH, Fang C, Lam ACC, Zhang YY. Numerical study and practical design of beam-to-column connections with shape memory alloys. Journal of Constructional Steel Research 2015;104:177-192.

[6] Speicher MS, Desroches R, Leon RT. Experimental results of a NiTi shape memory alloy (SMA)-based recentering beam-column connection. Engineering Structures 2011;33(9):2448-2457.

[7] Wang W, Fang C, Liu J. Self-centering beam-to-column connections with combined superelastic SMA bolts and steel angles. Journal of Structural Engineering ASCE 2017;143(2):04016175.

[8] Qiu C, Zhu S. Shake table test and numerical study of self-centering steel frame with SMA braces. Earthquake Engineering and Structural Dynamic 2017;46(1):117-137.

[9] Fang C, Wang W, He C, Chen YY. Self-centring behaviour of steel and steel-concrete composite connections equipped with NiTi SMA bolts. Engineering Structures 2017;150:390-408.

[10] Wang W, Fang C, Yang X, Chen YY, Ricles J, Sause R. Innovative use of a shape memory alloy ring spring system for self-centering connections. Engineering Structures 2017;153:503-515.

[11] Dolce M, Cardone D. Mechanical behaviour of shape memory alloys for seismic applications 2. Austenite NiTi wires subjected to tension. International Journal of Mechanical Sciences 2001;43(11):2657-2677.

[12] DesRoches R, McCormick J, Delemont MA. Cyclic properties of superelastic shape memory alloy wires and bars. Journal of Structural Engineering 2004;130(1):38-46.

[13] Fugazza D. Experimental investigation on the cyclic properties of superelastic NiTi shape-memory alloy wires and bars. Rose School, European school for advanced studies in reduction of seismic risk, Pavia, 2005.

[14] Fang C, Yam MCH, Chan TM, Wang W, Yang X, Lin X. A study of hybrid self-centring connections equipped with shape memory alloy washers and bolts. Engineering Structures 2018;164:155-168.

[15] MA Savi, PMCL Pacheco, MS Garcia, RAA Aguiar, LFG De Souza, et al. Nonlinear geometric influence on the mechanical behavior of shape memory alloy helical springs. Smart Materials & Structures 2015;24(3):035012.

[16] Fang C, Yam MCH, Ma HW, Chung KF. Tests on superelastic Ni–Ti SMA bars under cyclic tension and direct-shear: towards practical recentering connections. Materials & Structures 2015;48(4):1013-1030.

[17] Fang C, Yam MCH, Lam ACC, Zhang YY. Feasibility study of shape memory alloy ring spring systems for self-centering seismic resisting devices. Smart Materials and Structures 2015;24:075024.

[18] Fang C, Wang W, Ricles J, Yang X, Zhong Q, Sause R, Chen Y. Application of an Innovative SMA Ring Spring System for Self-Centering Steel Frames Subject to Seismic Conditions. Journal of Structural Engineering 2018;144(8):04018114.

[19] Reedlunn B, Daly S, Shaw J. Superelastic shape memory alloy cables: Part I–isothermal tension experiments. International Journal of Solids and Structures 2013;50(20-21):3009-3026.

[20] Ozbulut OE, Daghash S, Sherif MM. Shape memory alloy cables for structural applications[J]. Journal of Materials in Civil Engineering 2015;28(4):04015176.

[21] Sherif MM, Ozbulut OE. Tensile and superelastic fatigue characterization of NiTi shape memory cables. Smart Materials and Structures 2018;27(1):015007.

[22] Carboni B, Lacarbonara W, Auricchio F. Hysteresis of multiconfiguration assemblies of nitinol and steel strands: experiments and phenomenological identification. Journal of Engineering Mechanics 2014;141(3):04014135.

[23] Biggs DB, Shaw JA. Experimental characterization of shape memory alloy actuator cables. Proc. SPIE 9800, Behavior and Mechanics of Multifunctional Materials and Composites 2016.

[24] Mas B, Biggs D, Vieito I, Cladera A, Shaw J, Martínez-Abella F. Superelastic shape memory alloy cables for reinforced concrete applications. Construction and Building Materials 2017;148:307-320.

[25] Sun S, Lv M. Dynamic response of a high-rise chemical tower controlled by pseudo-elastic shape memory alloy cables. Journal of Intelligent Material Systems and Structures 2016;27(10): 1412-1422.

[26] Zheng Y, Dong Y, Li Y. Resilience and life-cycle performance of smart bridges with shape memory alloy (SMA)-cable-based bearings. Construction and Building Materials 2018;158:389-400.

[27] Frick CP, Ortega AM, Tyber J, Maksound AElM, Maier HJ, Liu YN, Gall K. Thermal processing of polycrystalline NiTi shape memory alloys. Materials Science and Engineering: A 2005;405(1-2):34-49.

[28] Tyber J, McCormick J, Gall K, DesRoches R, Maier JH, Abdel Maksoud AE. Structural engineering with NiTi. I: Basic materials characterization. Journal of Engineering Mechanics 2007;133(9):1009-1018.

[29] McCormick J, Tyber J, DesRoches R, Gall K, Maier HJ. Structural engineering with NiTi. II: Mechanical behavior and scaling. Journal of Engineering Mechanics 2007;133(9):1019-1029.

[30] Sadiq H, Wong MB, Al-Mahaidi R, Zhao XL. The effects of heat treatment on the recovery stresses of shape memory alloys. Smart Materials and Structures 2010;19(3):035021.

[31] Huang X, Liu Y. Effect of annealing on the transformation behavior and superelasticity of NiTi shape memory alloy. Scripta Materialia 2001;45(2):153-160.

[32] Wang W, Fang C, Liu J. Large size superelastic SMA bars: heat treatment strategy, mechanical property and seismic application. Smart Materials and Structures 2016;25(7):075001.

[33] Sutton MA, Orteu JJ, Schreier HW. Image Correlation for Shape, Motion, and Deformation Measurements: Basic Concepts, Theory, and Applications. Springer, New York, 2009.

[34] Reedlunn B, Daly S, Shaw J. Superelastic shape memory alloy cables: Part II–Subcomponent isothermal responses. International Journal of Solids and Structures 2013;50(20-21):3027-3044.

[35] Introduction to Nitinol. Memry Corporation 2017, 3 Berkshire Boulevard, Bethel, CT 06801, www.memry.com.

[36] Liang C, Rogers C. One-Dimensional Thermomechanical Constitutive Relations for Shape Memory Materials. Journal of Intelligent Material Systems & Structures 1990;1(2):207-234.

[37] Brinson LC. One-Dimensional Constitutive Behavior of Shape Memory Alloys: Thermomechanical Derivation with Non-Constant Material Functions and Redefined Martensite Internal Variable 1993;2(2):229-242.

[38] Auricchio F, Taylor RL. Shape-memory alloys: modelling and numerical simulations of the finite-strain superelastic behavior. Computer Methods in Applied Mechanics & Engineering 1997;143(1):175-194.

[39] Mazzoni S, McKenna F, Scott M, Fenves G. Open system for earthquake engineering simulation (OpenSees). User command language manual, Pacific Earthquake Engineering Research Center, University of California, Berkeley, 2006.

[40] Barbato M, Conte JP. Finite element structural response sensitivity and reliability analyses using smooth versus non-smooth material constitutive models. International Journal of Reliability and Safety 2006;1(1-2):3-39.

[41] Scott BD, Park P and Priestley MJN. Stress-strain behavior of concrete confined by overlapping hoops at low and high strain rates. Journal of American Concrete Institute 1982;79(1):13-27.

[42] California Department of Transportation (CLATRANS). Seismic design criteria, Version 1.6, Sacramento, California, 2010.

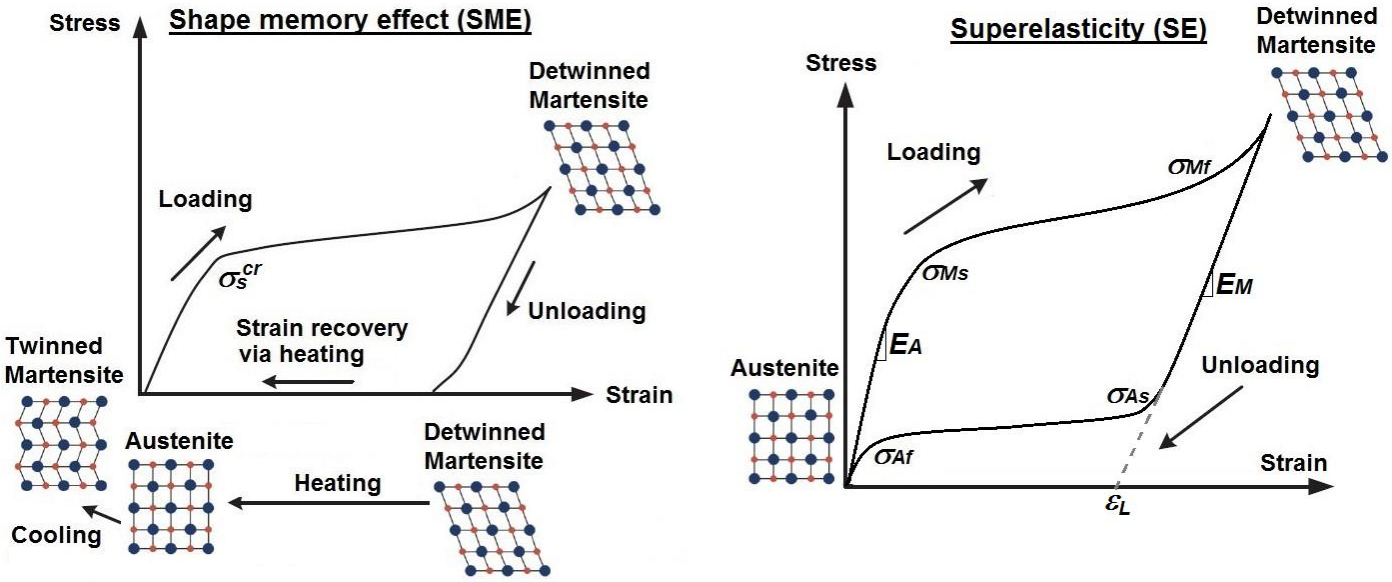

Fig. 1 Basic stress-strain responses of SMA exhibiting SME or SE

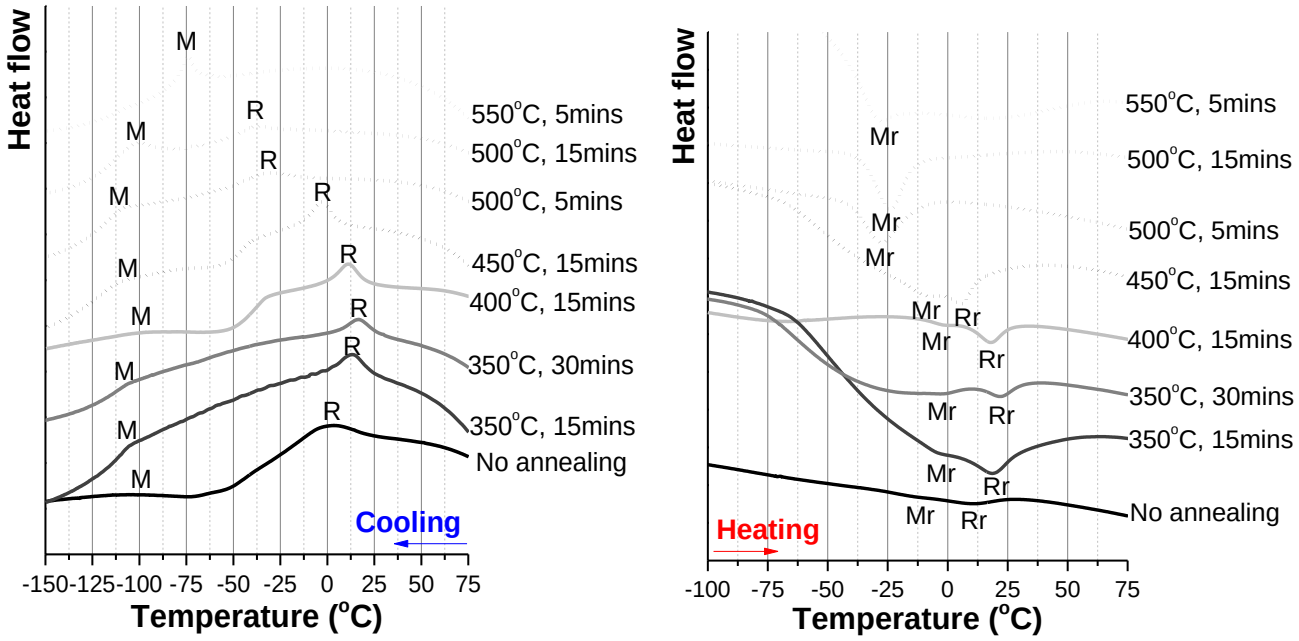

(a)

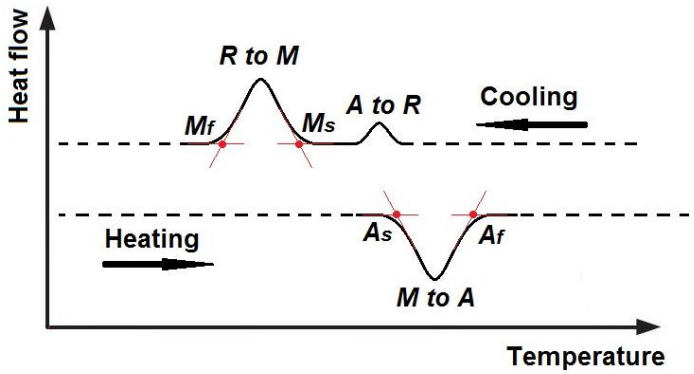

(b)

Fig. 2 DSC curves: a) results of wire samples after being subjected to different annealing schemes (in the subfigure, "R" represents forward transformation from A to R phases; "M" represents forward transformation from R or A to M phases; "Mr" represents reverse transformation from M to R or A phases; "Rr" represents reverse transformation from R to A phases); b) illustration of DSC reading

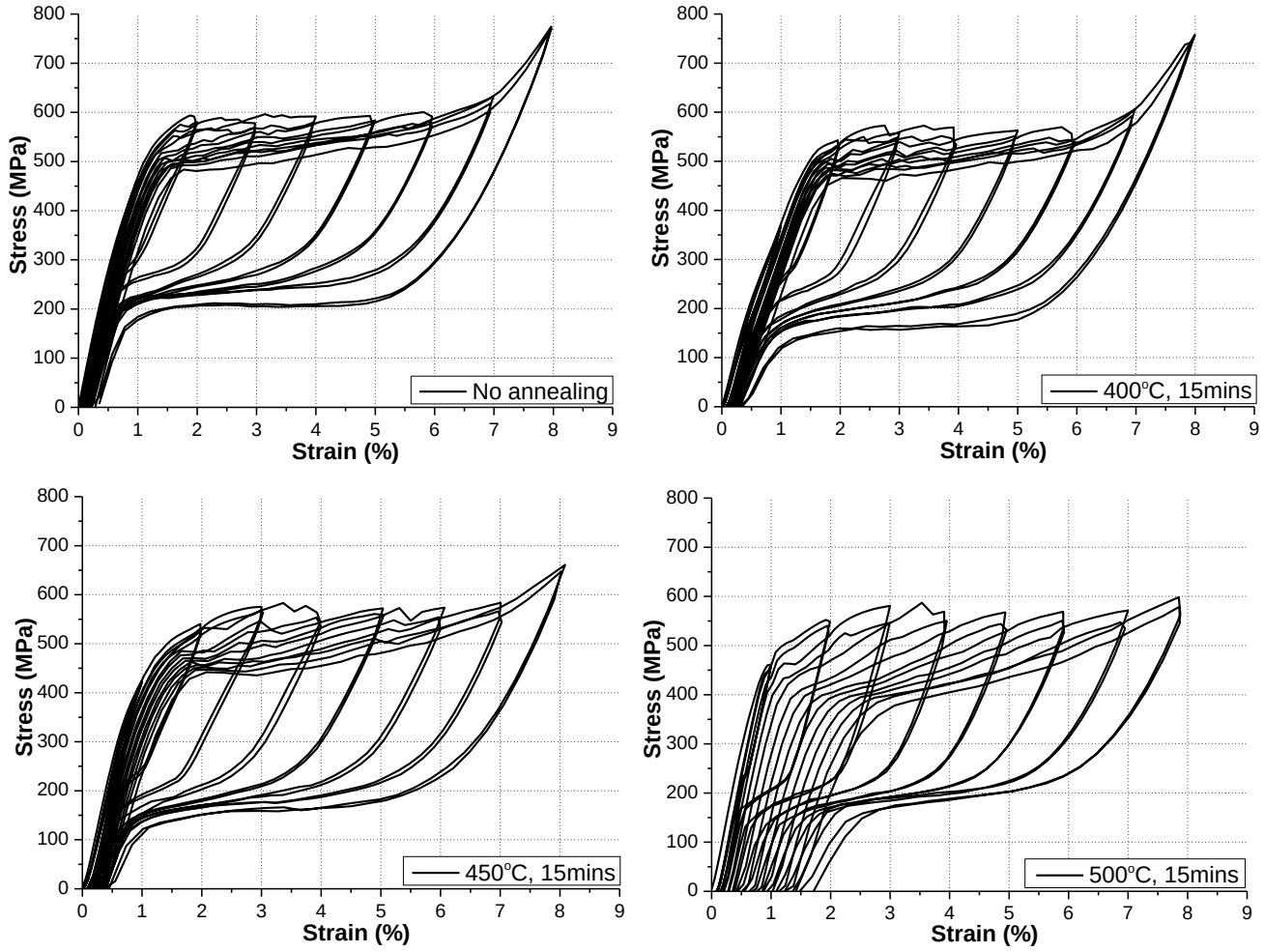

Fig. 3 Influence of annealing on stress-strain responses of monofilament SMA wire samples

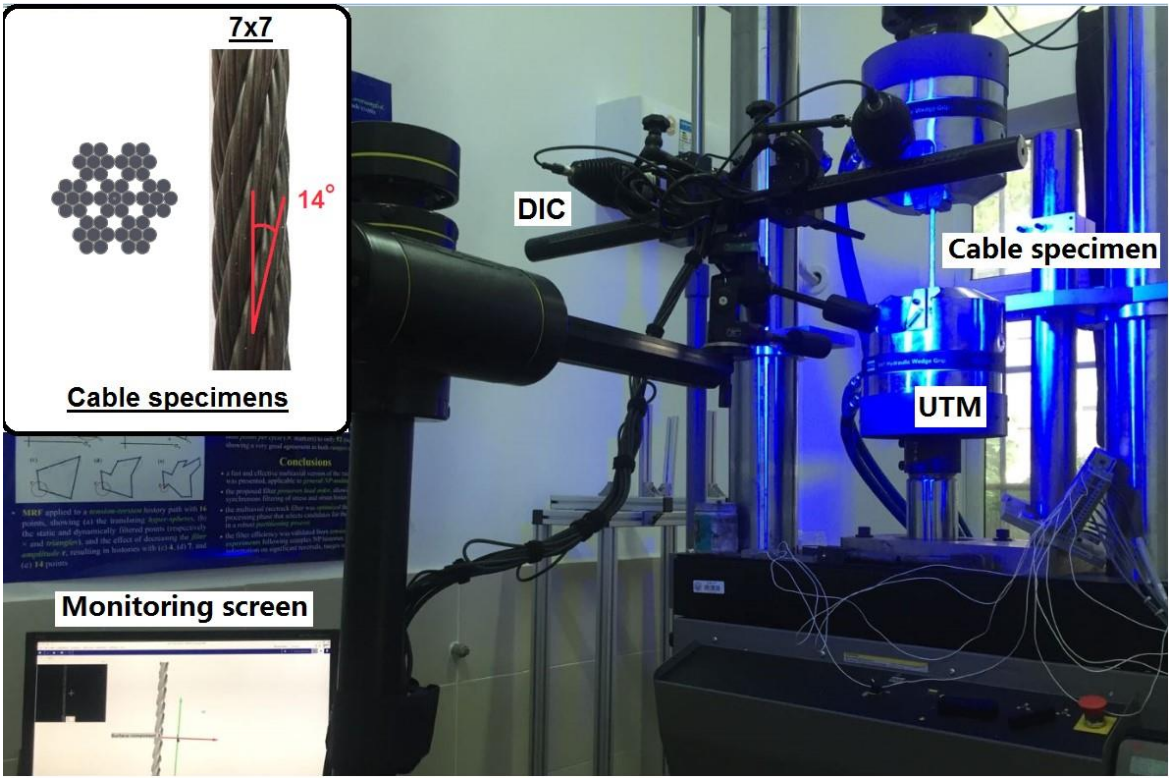

Fig. 4 Details of SMA cable specimen and test setup

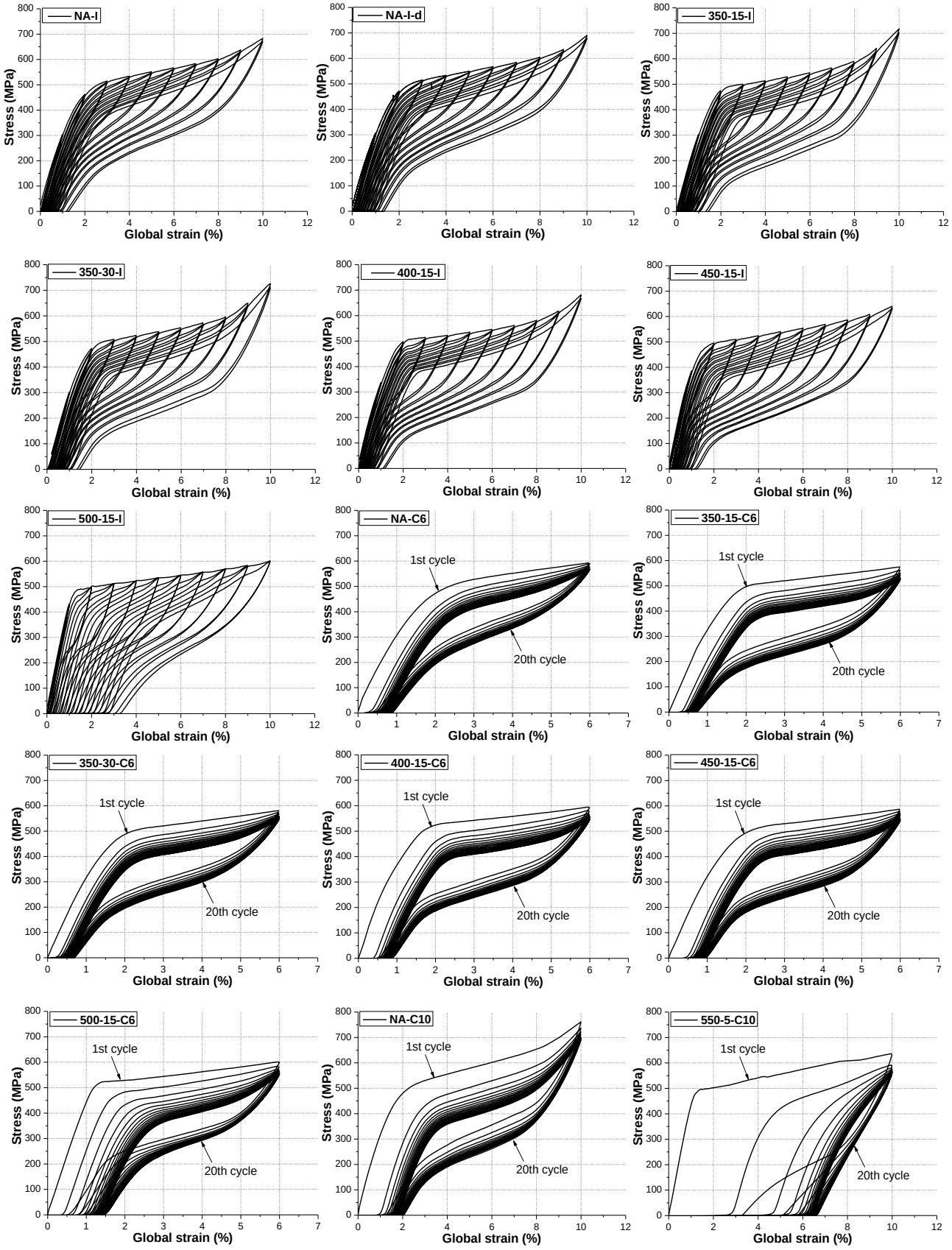

Fig. 5 Hysteretic behavior of SMA cables specimens

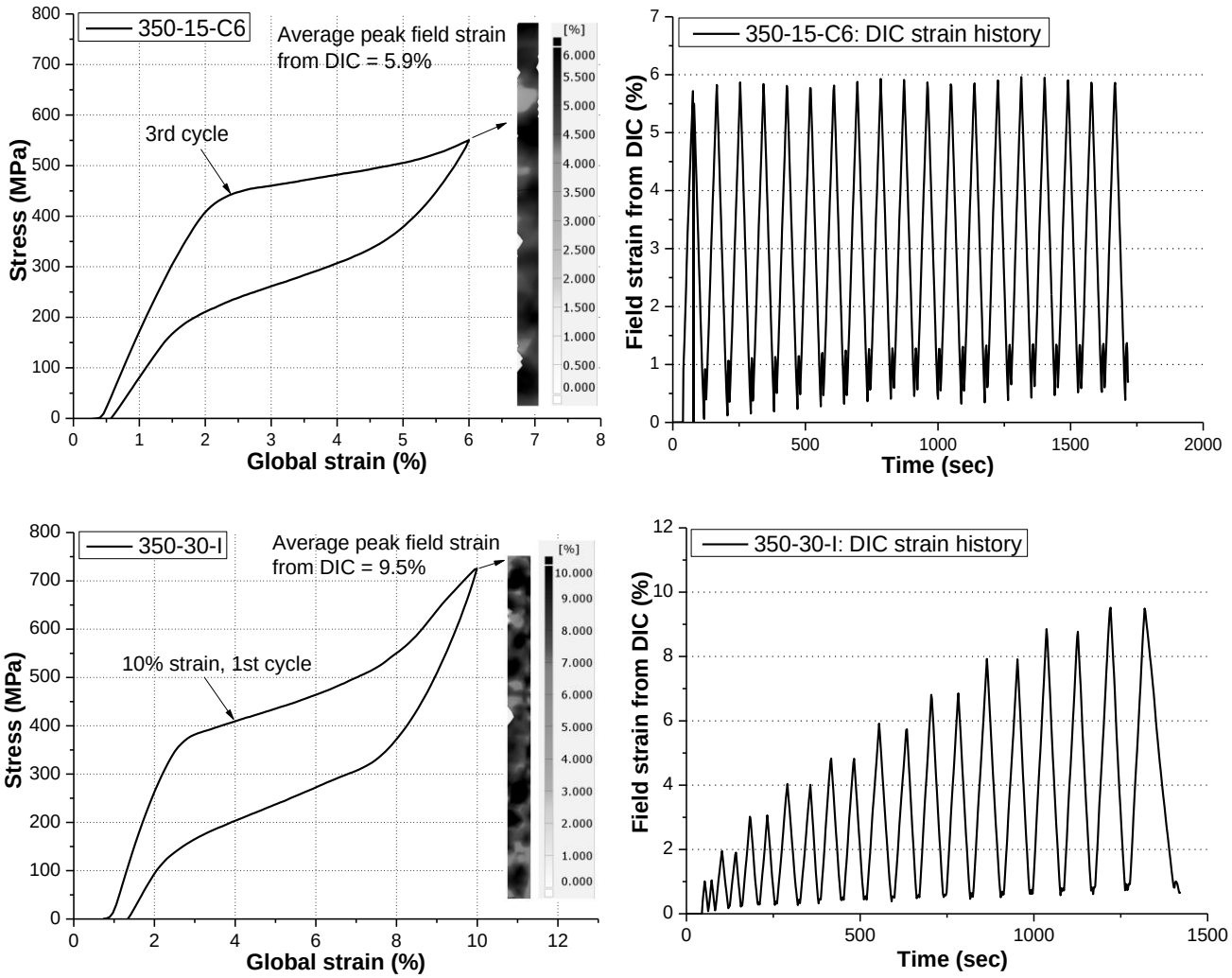

Fig. 6 Typical local strain field from DIC

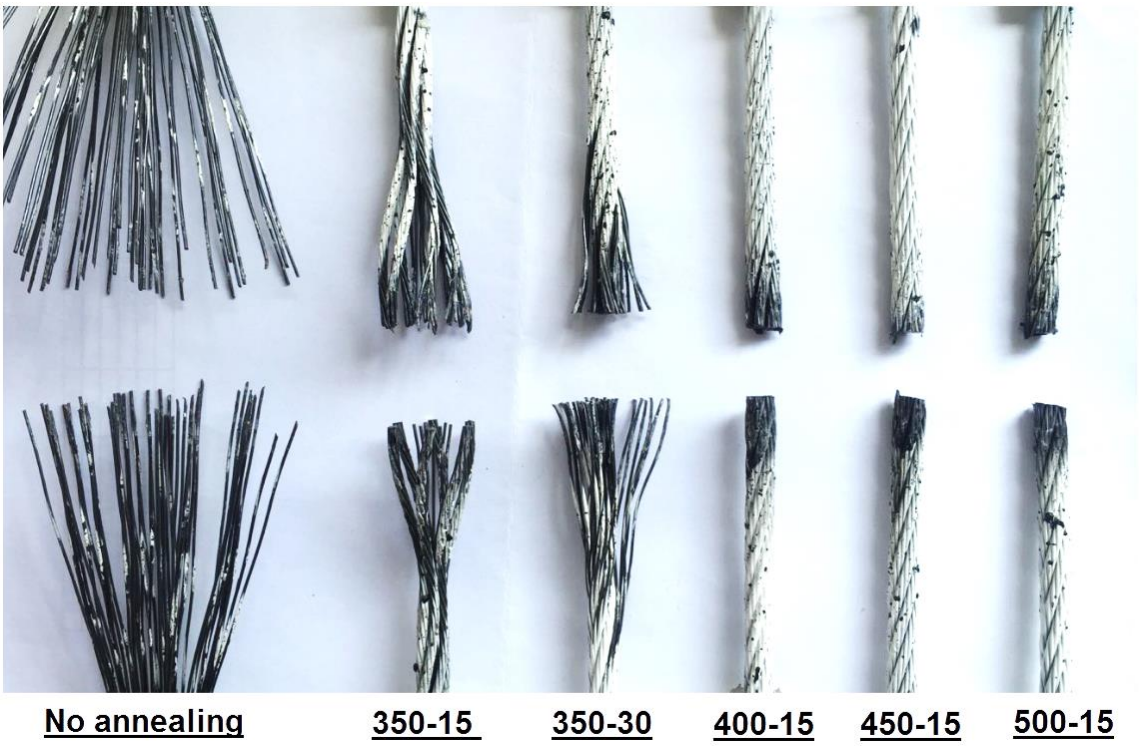

Fig. 7 Form setting ability of SMA cables subjected to varying annealing schemes

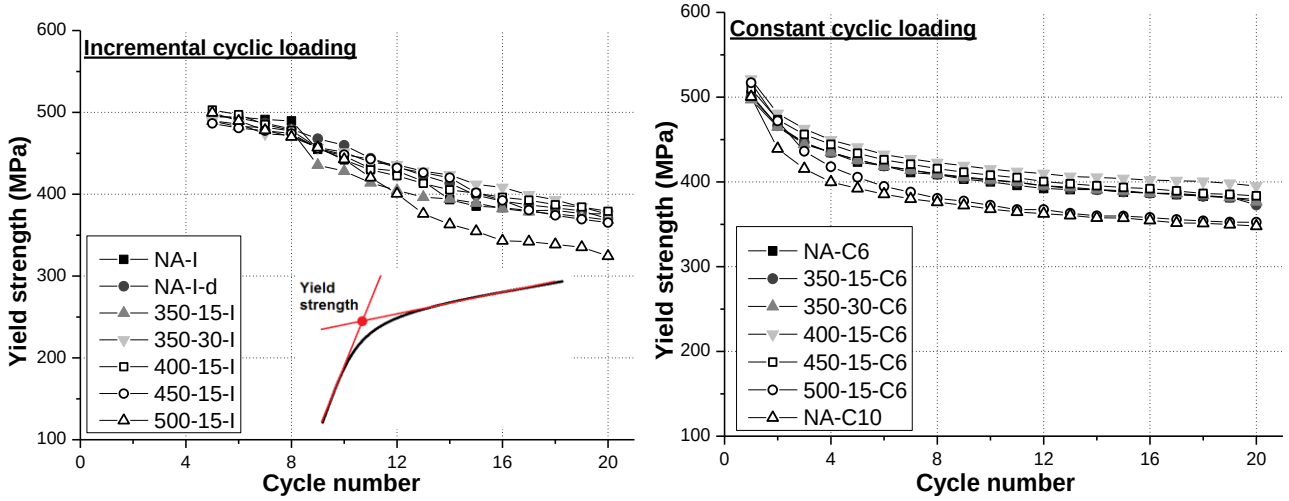

(a)

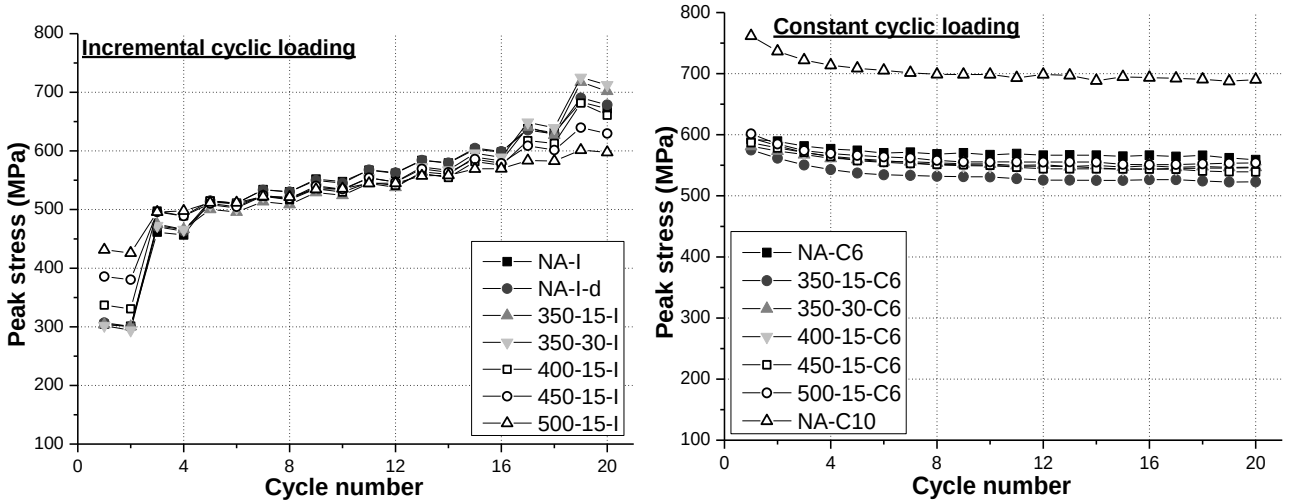

(b)

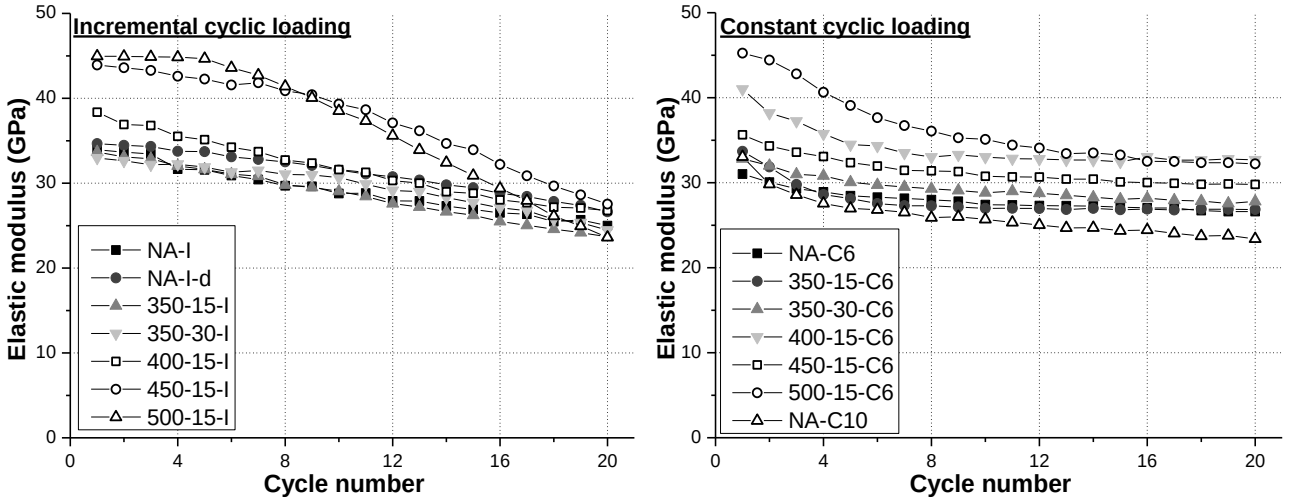

(c)

Fig. 8 Strength and stiffness properties of SMA cable specimens: a) yield strength, b) peak stress, c) elastic modulus

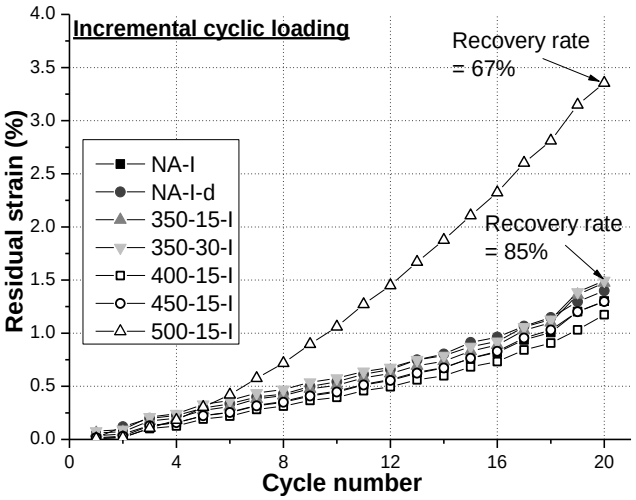

(a)

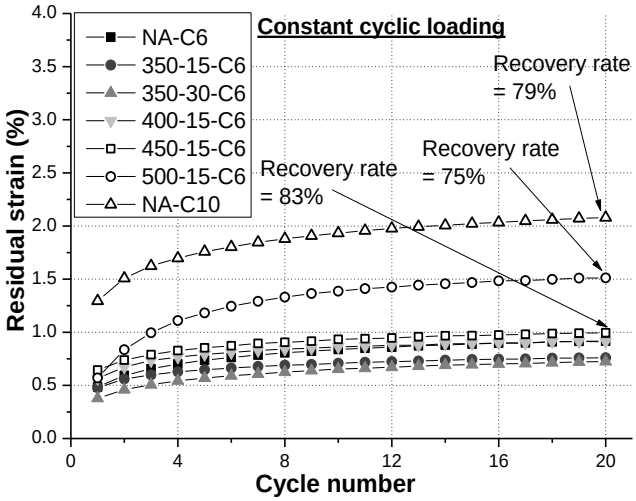

(b)

Fig. 9 Self-centering capability of SMA cable specimens: a) incremental cyclic loading, b) constant cyclic loading

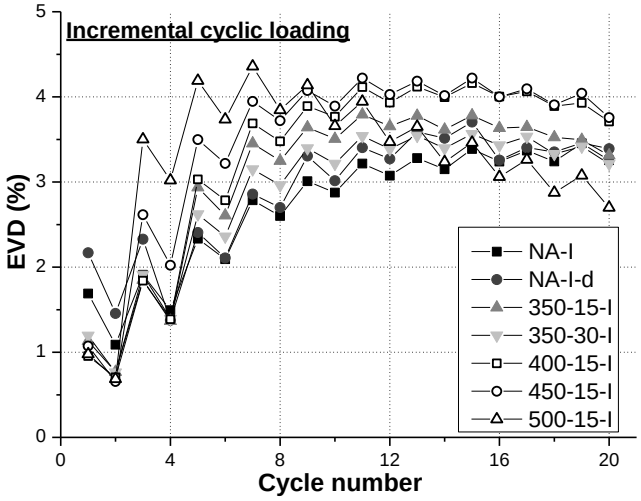

(a)

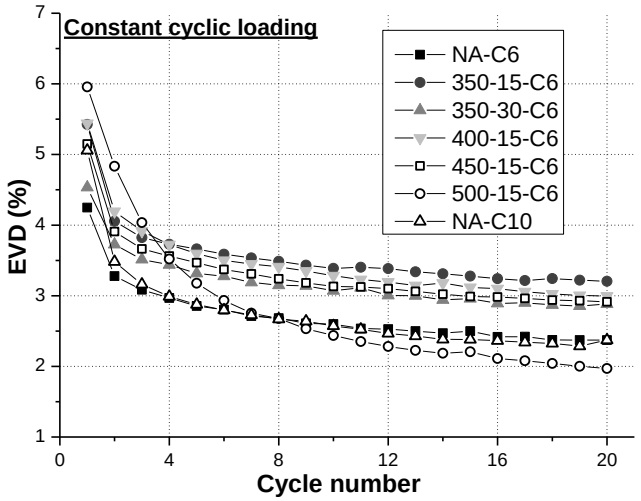

(b)

Fig. 10 Energy dissipation characteristic of SMA cable specimens: a) incremental cyclic loading, b) constant cyclic loading

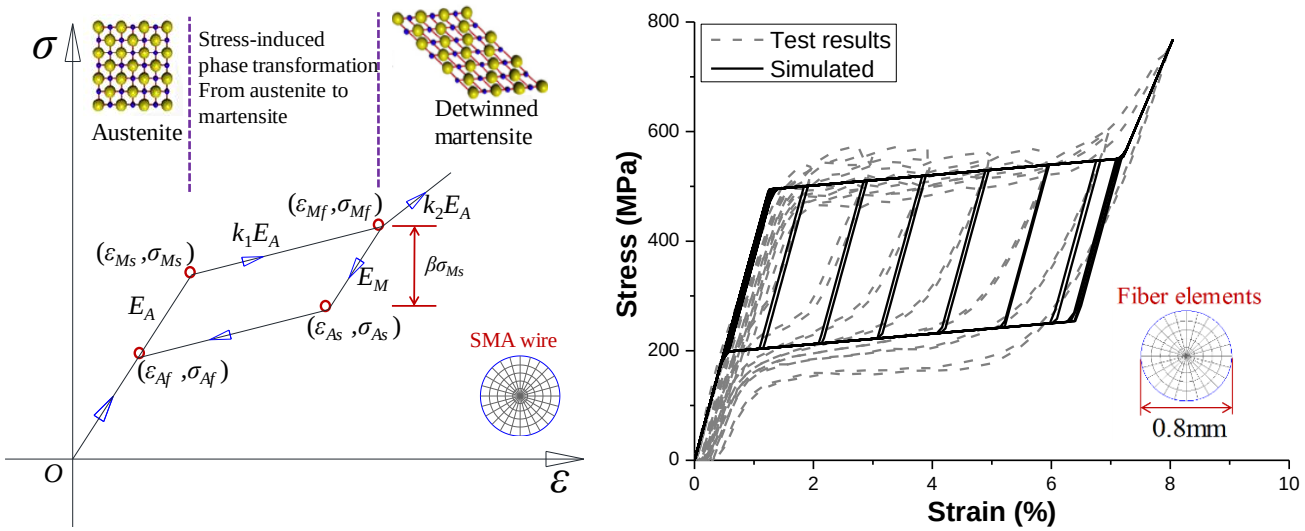

Fig. 11 Modelling of monofilament SMA wires

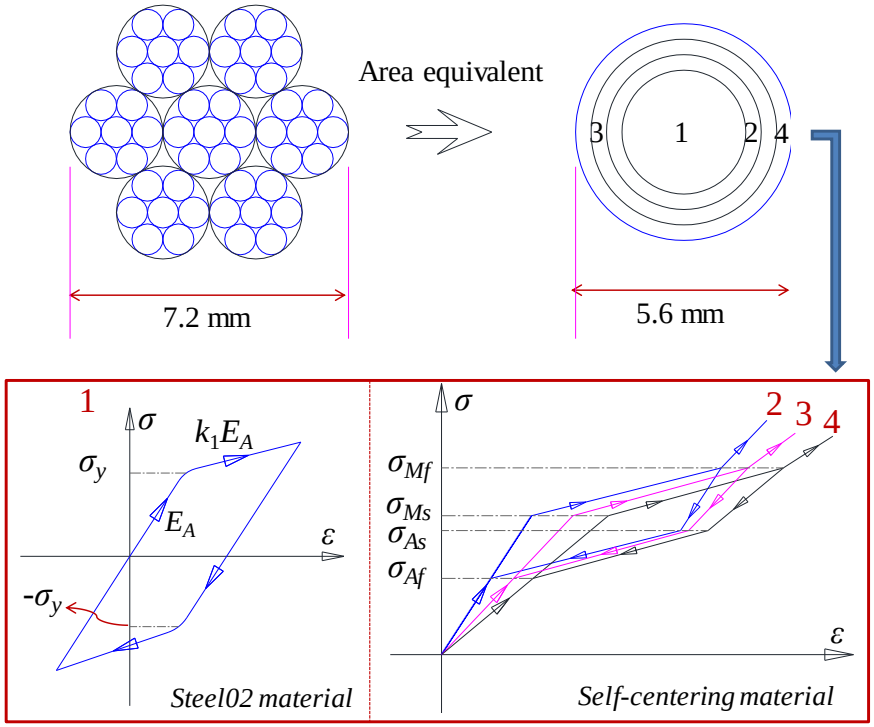

(a)

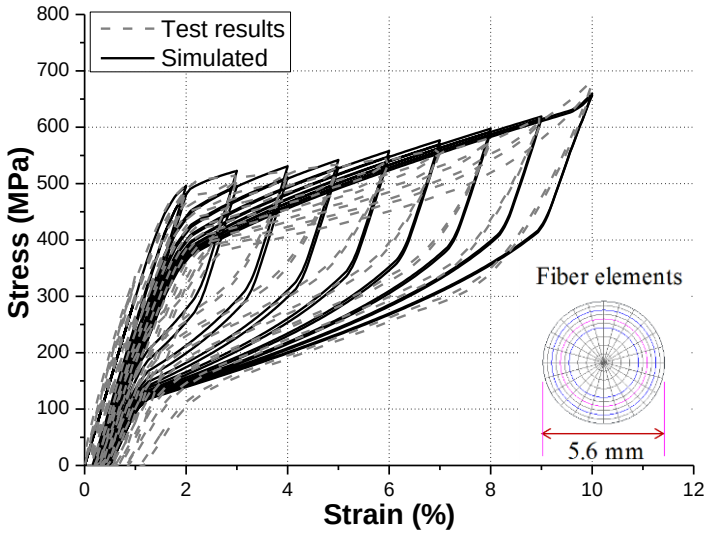

(b)

Fig. 12 Modelling of SMA cable: a) modelling strategy, b) comparison between test and simulated results

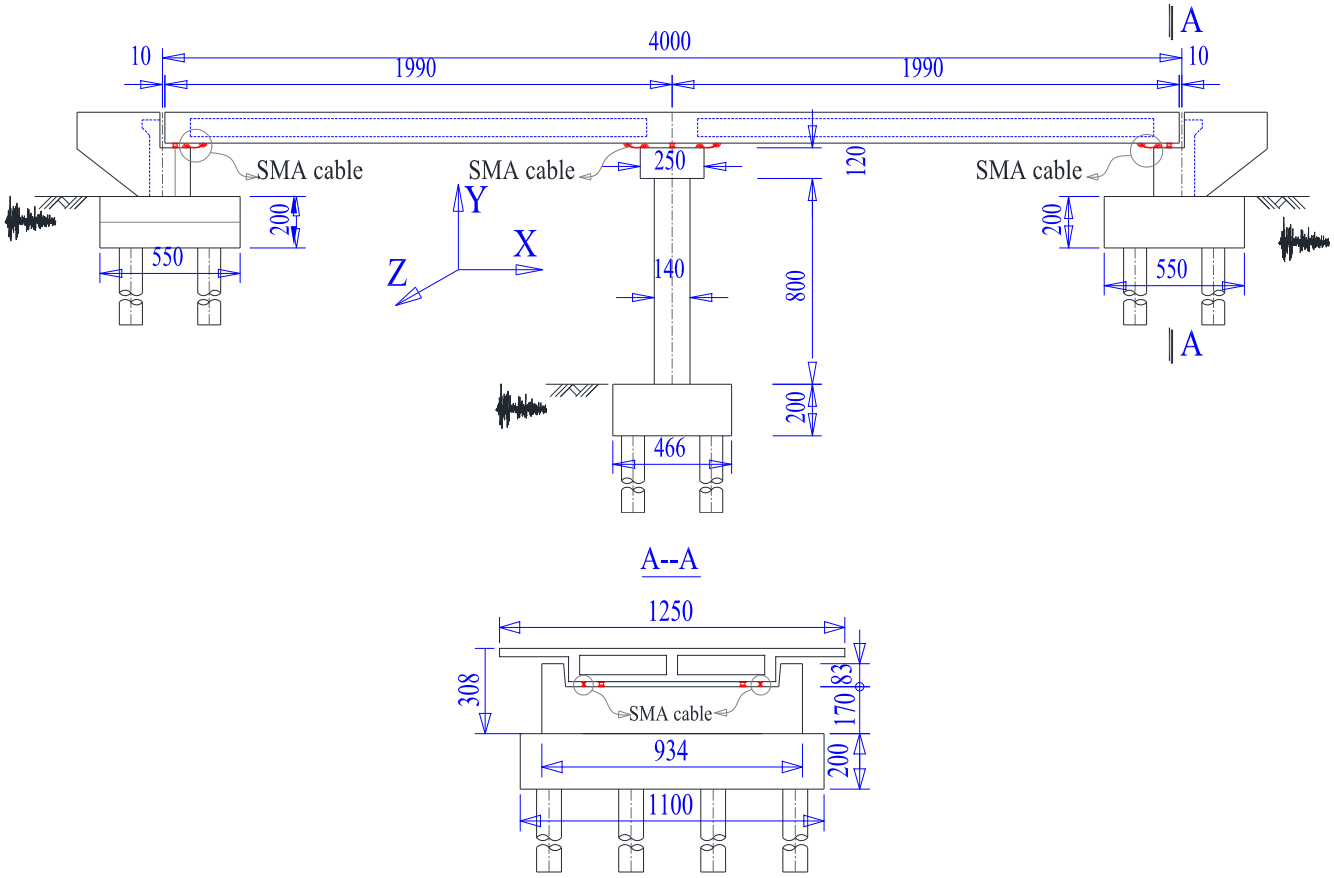

Fig. 13 Configuration of RC bridge with SMA cable restrainers (unit: cm)

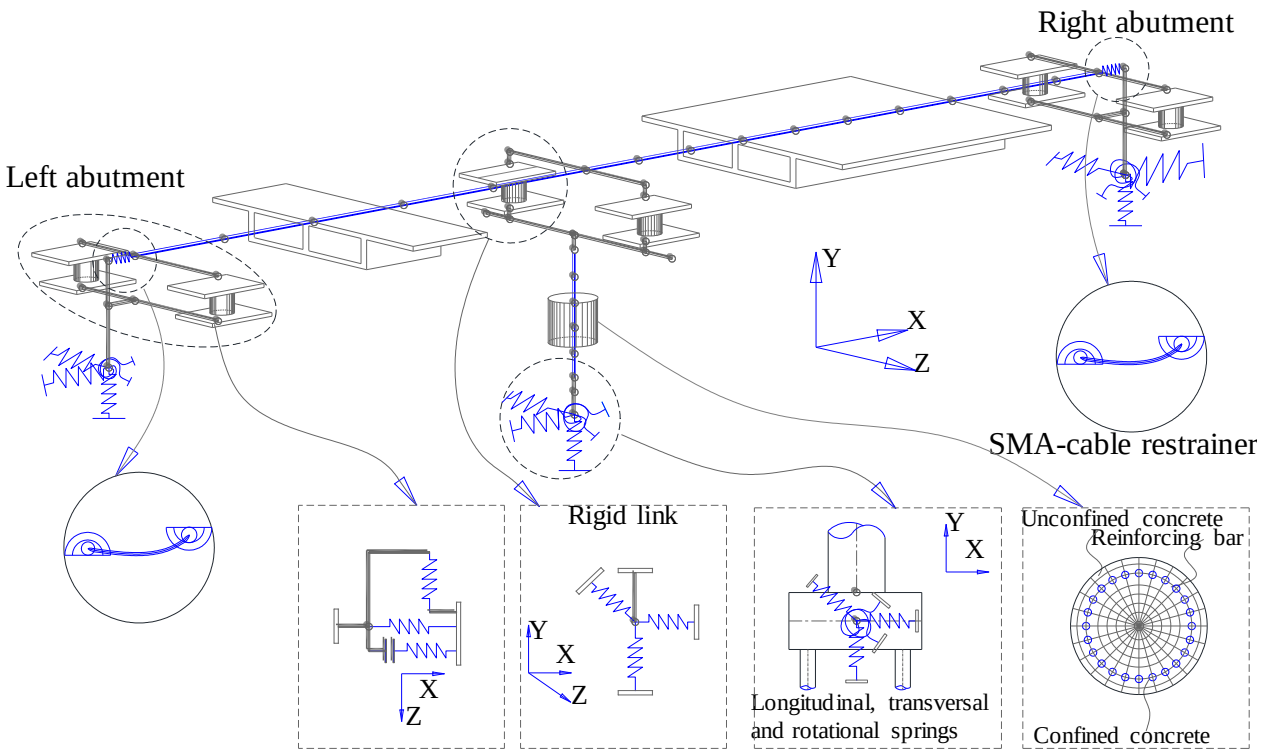

(a)

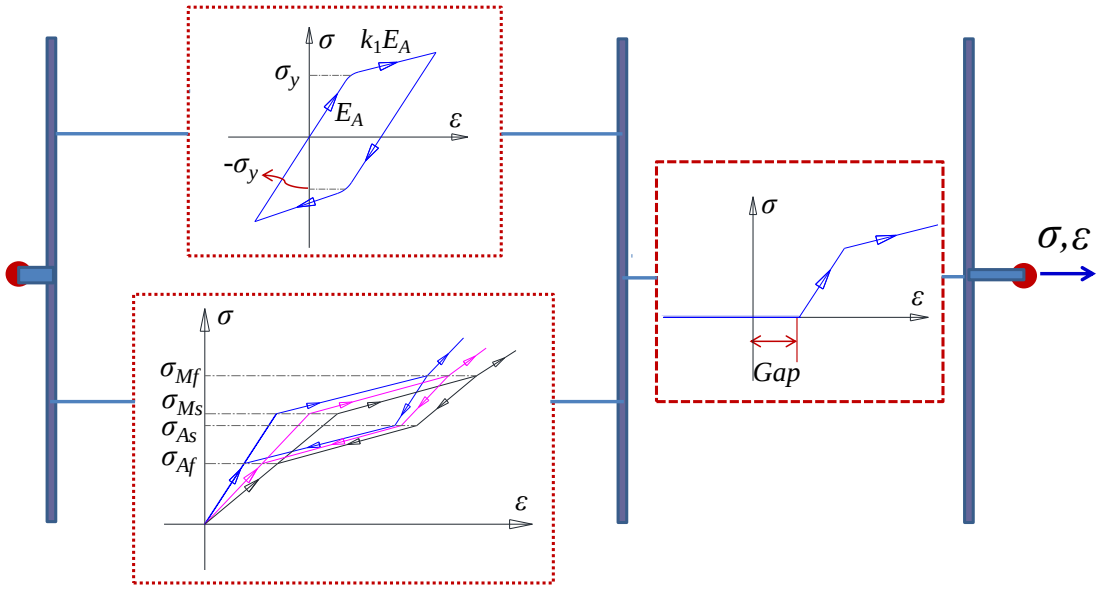

(b)

Fig. 14 FE model of RC bridge with SMA cable restrainer: a) schematic illustration of bridge model; b) modelling of slack SMA cable

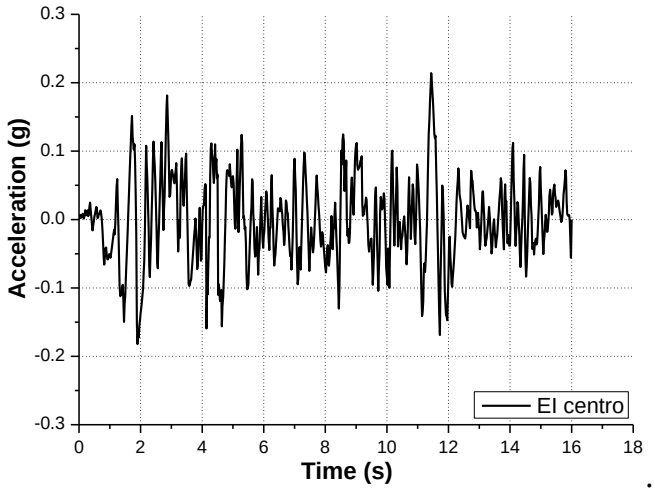

(a)

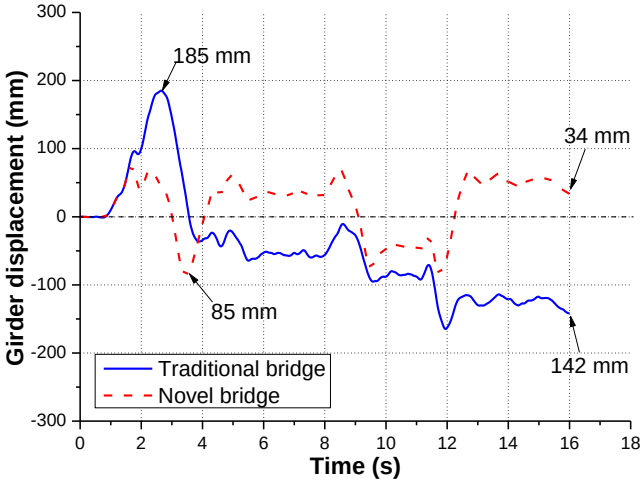

(b)

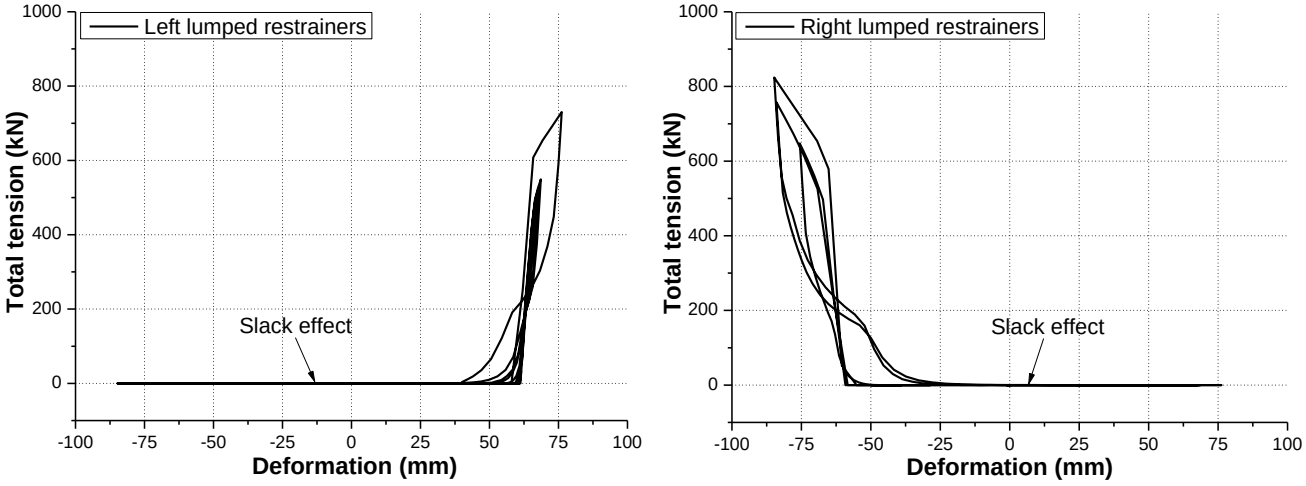

(c)

Fig. 15 Case study: a) accelerogram of El Centro (EW) earthquake; b) displacement response of girder, c) total tension force vs. deformation of SMA-cable restrainers

Table 1 Details of SMA cable specimens

Designation	Annealing temperature (°C)	Duration (mins)	Loading protocol	Maximum global strain
NA-I	N/A	N/A	Incremental	10%
NA-I-d	N/A	N/A	Incremental	10%
350-15-I	350	15	Incremental	10%
350-30-I	350	30	Incremental	10%
400-15-I	400	15	Incremental	10%
450-15-I	450	15	Incremental	10%
500-15-I	500	15	Incremental	10%
NA-C6	N/A	N/A	Constant	6%
350-15-C6	350	15	Constant	6%
350-30-C6	350	30	Constant	6%
400-15-C6	400	15	Constant	6%
450-15-C6	450	15	Constant	6%
500-15-C6	500	15	Constant	6%
NA-C10	N/A	N/A	Constant	10%
550-5-C10	550	5	Constant	10%

Table 2 Key parameters of monofilament SMA wire

Strain		Stress (MPa)		k_2	β
ε_{Ms}	0.0125	σ_{Ms}	500.0	0.65	0.6
ε_{Mf}	0.072	σ_{Mf}	557.1		
ε_{As}	0.0645	σ_{As}	257.1		
ε_{Af}	0.005	σ_{Af}	200.0		

Table 3 Key parameters of SMA cable

Material No.	Material Name	Key parameters							
		Yielding strength (MPa)	E_A (GPa)	k_0	k_1	k_2	E_M (GPa)	Area (mm^2)	β
1	Steel02	σ_y = 500	36	0.9	0.06			8.0	
2	Self-centering	σ_{Ms} = 500	32	0.8	0.06	0.65	32	4.5	0.40
3	Self-centering	σ_{Ms} = 500	28	0.7	0.06	0.65	28	5.5	0.40
4	Self-centering	σ_{Ms} = 500	24	0.6	0.06	0.65	24	6.5	0.40